# Microfluidic Chemotaxis Platform for Differentiating the Roles of Soluble and Bound Amyloid-ß on Microglial Accumulation

SCIENTIFIC REPORTS

OPEN

SUBJECT AREAS:
ASSAY SYSTEMS
ALZHEIMER'S DISEASE
BIOMEDICAL ENGINEERING
NEUROIMMUNOLOGY

Received
18 January 2013

Accepted
23 April 2013

Published
10 May 2013

Correspondence and requests for materials should be addressed to D.I. (dirimia@hms.harvard.edu)

# Microfluidic Chemotaxis Platform for Differentiating the Roles of Soluble and Bound Amyloid-$\beta$ on Microglial Accumulation

Hansang Cho[1], Tadafumi Hashimoto[2], Elisabeth Wong[1], Yukiko Hori[2], Levi B. Wood[3], Lingzhi Zhao[2,4], Kevin M. Haigis[3], Bradley T. Hyman[2] & Daniel Irimia[1]

[1]BioMEMS Resource Center, Massachusetts General Hospital, Harvard Medical School, [2]MassGeneral Institute for Neurodegenerative Disease, Massachusetts General Hospital, Harvard Medical School, [3]Molecular Pathology Unit, Massachusetts General Hospital, Harvard Medical School, [4]Appel Alzheimer's Disease Research Institute, Department of Neurology and Neuroscience, Weill Cornell Medical College.

**Progressive microglial accumulation at amyloid-$\beta$ ($A\beta$) plaques is a well-established signature of the pathology of Alzheimer's disease, but how and why microglia accumulate in the vicinity of $A\beta$ plaques is unknown. To understand the distinct roles of $A\beta$ on microglial accumulation, we quantified microglial responses to week-long lasting gradients of soluble $A\beta$ and patterns of surface-bound $A\beta$ in microfluidic chemotaxis platforms. We found that human microglia chemotaxis in gradients of soluble $A\beta_{42}$ was most effective at two distinct concentrations of 23 pg.mL$^{-1}$ and 23 ng.mL$^{-1}$ $A\beta_{42}$ in monomers and oligomers. We uncovered that while the chemotaxis at higher $A\beta$ concentrations was exclusively due to $A\beta$ gradients, chemotaxis at lower concentrations was enhanced by $A\beta$-induced microglial production of MCP-1. Microglial migration was inhibited by surface-bound $A\beta_{42}$ in oligomers and fibrils above 45 pg.mm$^{-2}$. Better understanding of microglial migration can provide insights into the pathophysiology of senile plaques in AD.**

Microglial cells are resident macrophages in the central neural system (CNS) and have multiple functions in normal and pathological brains[1–6]. Ramified microglia are believed to constantly scan the brain and clear the CNS of toxic agents and debris[7,8]. In the context of Alzheimer's disease (AD), diminished clearance of $A\beta$ due to impaired microglia is postulated to be one of the mechanisms of $A\beta$ plaque formation[9]. Once $A\beta$ forms plaques, microglia become hyper-activated[10], accumulate around the plaques, and consequently secrete neurotoxic agents including neuroinflammatory mediators, reactive oxygen species, and free radicals[11–14]. Understanding the mechanisms that lead to microglial accumulation and inflammatory responses may provide useful insights into developing strategies for AD treatment. However, several studies report different interactions between microglia and other factors[15–17]. Previous *in vivo* studies of microglia migration were hampered by both the inability to observe long-term effects of $A\beta$ on microglia[18] and the complexity of senile plaques, which are deposits of oligomeric and fibrillar $A\beta$, surrounded by a "halo" of soluble oligomeric $A\beta$[19], activated glia, and dystrophic neurites[12]. Activated microglial cells take on various morphologies: rounded, ramified shapes, rods to amoeboids, which complicate the visual tracking of these cells individually. Furthermore, previous *in vitro* attempts to study rat microglia migration in the presence of short lived, damaged axons[20], could not establish long-lasting gradients and were not conclusive for differentiating slow accumulation of microglia from random navigation[21,22].

Here, we have developed a novel microfluidic chemotaxis platform to study the motility of microglia responding to various types of $A\beta$ in a regulated manner. The new platform models soluble and bound $A\beta$ environments in AD brains and enables us to measure the distinct effects of both gradients of soluble $A\beta$, lasting longer than a week and surface-bound patterns of $A\beta$ on the migration of microglia.

## Results

**A microfluidic platform provides a gradient of soluble $A\beta$ and allows monitoring of microglial motility.** Based on *in vivo* observation of microglial accumulation on $A\beta$ plaques, we hypothesize that soluble $A\beta$ is an

effective stimulus in recruiting microglia, while insoluble, surface-bound $A\beta$ can capture the attracted microglia at the sites of surface-bound $A\beta$ (**Fig. 1a**). To understand how microglial migration is regulated by $A\beta$ in AD, we designed a unique microfluidic chemotactic platform composed of a large central reservoir (100 μL) supplying various types of soluble factors and two side reservoirs (100 μL each) containing medium. Human microglia were loaded in the annular (4 μL) compartment and their migration was observed towards the central (1 μL) compartment (**Fig. 1b–c**). The central and annular compartments were linked by migration channels ($10 \times 50 \times 500$ $\mu m^3$ in height, width, and length) forming gradients of soluble factors. Compared to a parallel configuration having equal surface areas for cell loading and cell collection, our axisymmetric configuration has a small central cell collecting compartment, which is smaller than a large annular cell loading compartment by a factor of 6. This enhances detection of recruitment. The long and thin migration channels can screen out unwanted entrance of inactivated microglia through mechanical constraints. Using this platform, we observed the migration of microglial cells, at single cell resolution, in real-time, for extended periods (**Fig. 1d**). We verified that refreshing media every two days allowed our experimental conditions to have a reasonable degree of physical and chemical stability of soluble $A\beta$ forms: 90 and 95% of original $A\beta$ gradients of monomeric and oligomeric soluble $A\beta$ for up to nine days (**Supplementary Fig. S1**), 74 and 84% of the total amounts of monomeric and oligomeric $A\beta$ solutions for two days (**Supplementary Fig. S2**). Thus, for most experiments, we refreshed media including soluble factors every two days. To evaluate the response of microglia to various types of $A\beta$, we tested 200 independent conditions at the same time, by imaging microglia in 8 plates, each with twenty-five platforms in an array format (**Supplementary Fig. S3**).

**Directional migration of microglia towards soluble *Aβ*.** To characterize the kinetics of microglial migration driven by soluble $A\beta$, we monitored individual microglial cells exposed to stable gradients of soluble $A\beta$ for four days using time-lapse microscopy. We observed that in the first 24 hours after introducing soluble $A\beta_{42}$ into a reservoir, microglia changed shape, became more elongated, and produced filopodia in random directions (**Fig. 2a, Supplementary Movies S1**). However, most of the cells remained stationary for the first 24 hours. Microglia started migrating on the second day of exposure to soluble $A\beta_{42}$ and migration was directional towards the soluble $A\beta_{42}$ reservoir (**Fig. 2b**). In the absence of soluble $A\beta_{42}$, microglia expanded their bodies but did not migrate during four-day experiments (**Supplementary Movies S2**). We measured comparable effects of monomeric and oligomeric forms, and measured a maximal migration speed of $5.1 \pm 4.2$ $\mu m.hr^{-1}$ at 23 $ng.mL^{-1}$ soluble monomeric $A\beta_{42}$ (**Fig. 2c**). We observed that microglia also entered the central compartment, the source of 2.3 $ng.mL^{-1}$ soluble $A\beta_{42}$ monomers (**Fig. 2d**). Additional quantification of the effect of soluble $A\beta$ on cellular distribution was performed by analyzing the changes in cellular density profile over time (**Fig. 2e**).

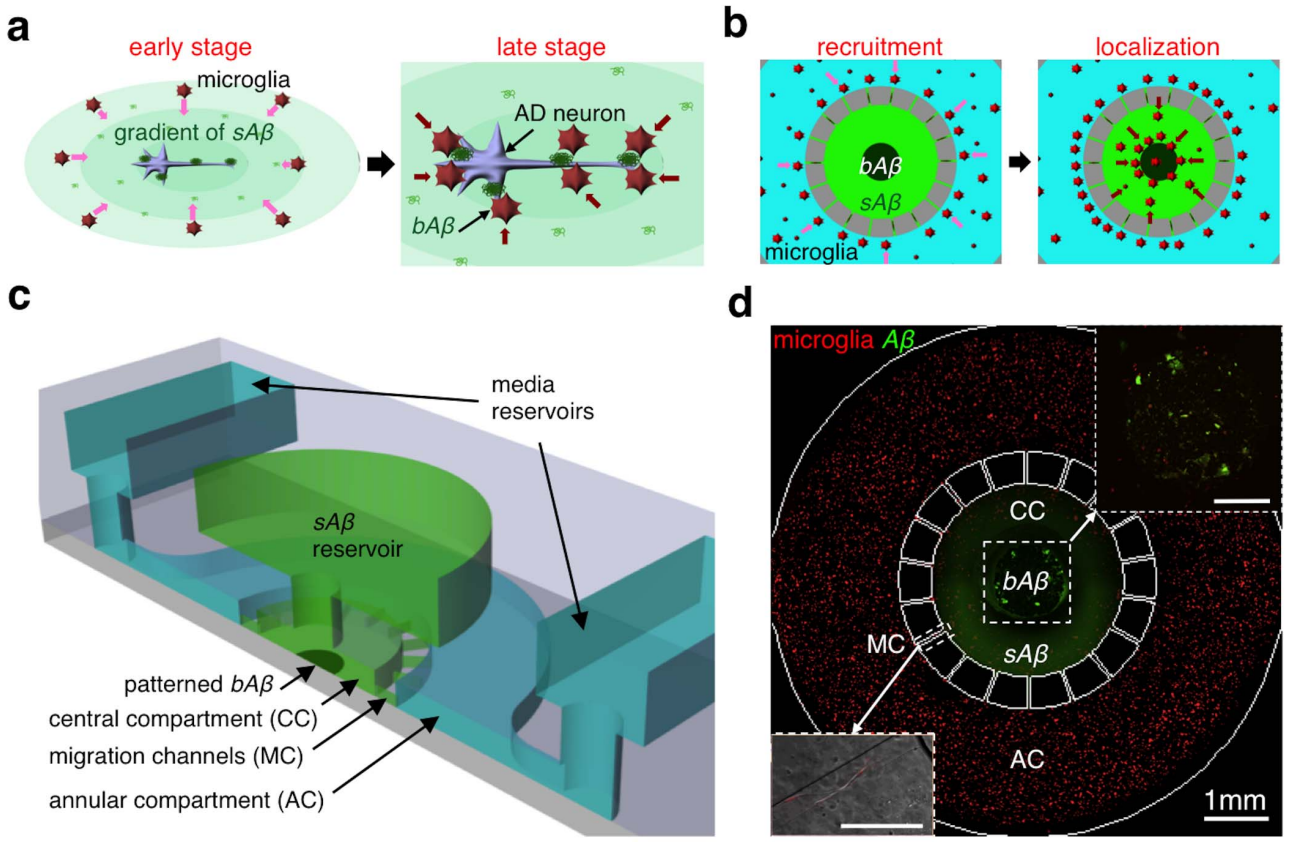


**Figure 1 | Replication of AD-*Aβ* environment in a microfluidic chemotaxis platform.** (a) We hypothesize that at early stages microglia are recruited by soluble $A\beta$ ($sA\beta$) (left) and at late stages co-localized with surface-bound $A\beta$ ($bA\beta$) near $A\beta$ plaques and neurons in AD brains (right). (b), (c) A microfluidic chemotaxis platform models the pathological $A\beta$ environments in AD brains and provides surface-bound $A\beta$ inside the central compartment (CC) and gradients of soluble $A\beta$ between the CC and the annular compartment (AC), along migration channels (MC). The axisymmetric configuration enhances the microglia counting during $A\beta$ recruitment and the long and thin migration channels help avoid counting errors due to spontaneous migration. (d) Fluorescent images show human microglia (red) inside the AC and soluble $A\beta$ (light green) and patterned $bA\beta$ (dark green) inside the CC. Microglia move in a gradient of $sA\beta$ between AC and CC, along the MC (left-lower inset). Microglia and $bA\beta$ co-localize in the CC after six days (right-upper inset). Scale bars, 200 μm.

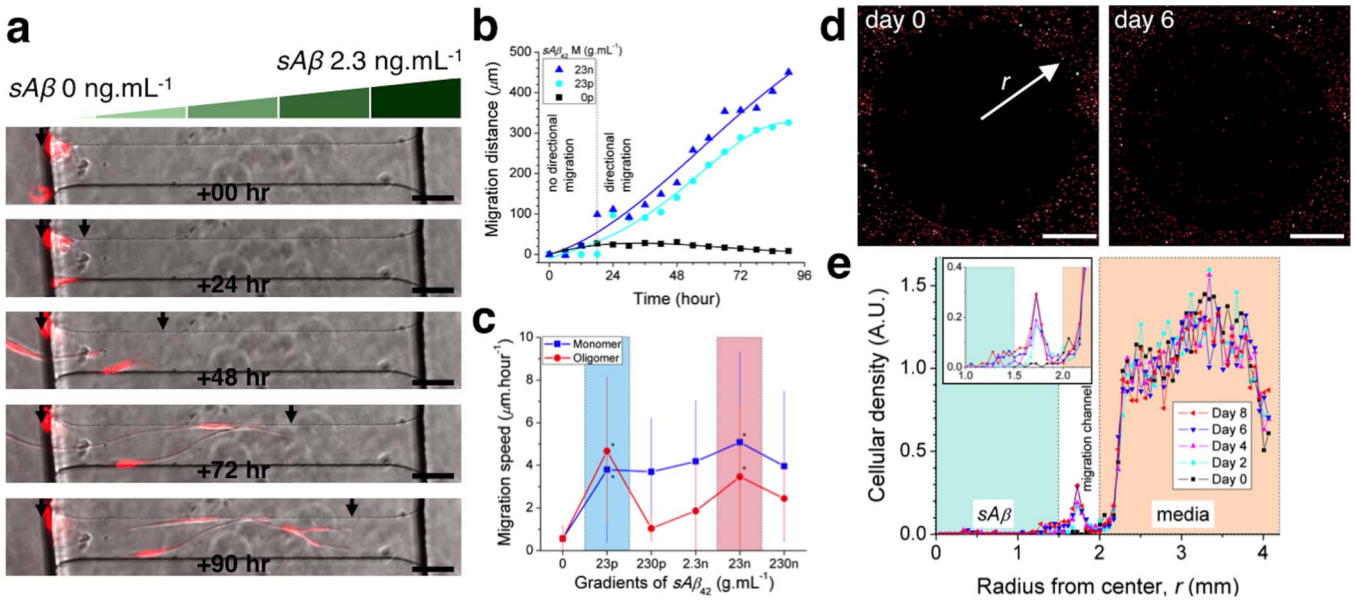


**Figure 2 | Inducement of microglial directional migration by gradients of soluble *Aβ*.** (a) Individual microglia migrate directionally along the gradient of *sAβ* monomers formed in migration channels. (b) Activation of directional motility can be discerned after 24 hours-exposure to gradients of $sA\beta_{42}$ in monomers at 23 pg.mL$^{-1}$ and 23 ng.mL$^{-1}$. (c) Dose-dependence of microglia migration speed during 4 days observations reveal two peak activities under gradients of soluble $A\beta_{42}$ monomers and oligomers at concentrations of 23 pg.mL$^{-1}$ and 23 ng.mL$^{-1}$ (ranges highlighted in cyan and pink colors, respectively). (d) Fluorescence images present detectable microglia accumulation toward the source of soluble $A\beta_{42}$ at day 6 compared to day 0. (e) Microglial density profiles at different days quantify the migration of microglia populations toward the source of soluble $A\beta_{42}$ in monomers at 2.3 ng.mL$^{-1}$. See the details on the stability and the preparation of soluble monomeric and oligomeric *Aβ* in Figs. S1, S2, and Supplementary methods. (Student's t-test. * $P < 0.01$ with respect to no $sA\beta_{42}$). $n_{cell} = 18$ for each condition. Data represent mean ± s.e.m.

To compare the effect of soluble *Aβ* in various forms and concentrations on microglial recruitment, we defined a recruitment index, *R.I.* (as defined in **Supplementary Methods**, **Supplementary Fig. S7**), representing the fraction of microglia cells recruited to the central compartment after loading soluble *Aβ* in the central compartment. We compared the *R.I.* values under various types of soluble $A\beta_{42}$ for eight days (**Fig. 3a, Supplementary Fig. S4**) and found that the *R.I.* value reached 5.0 ± 0.9 after exposure to monomeric synthetic $A\beta_{42}$ at 23 ng.mL$^{-1}$ and 4.0 ± 1.0 after exposure to oligomeric forms at 230 ng.mL$^{-1}$, on 'day 8' (**Fig. 3b**). Measuring the concentration dependence of directional migration speed and *R.I.* revealed two peaks of activity at two concentrations of soluble $A\beta_{42}$ that were three orders of magnitude apart (23 pg.mL$^{-1}$ and 23 ng.mL$^{-1}$) (**Fig. 2c and Fig. 3c**). Interestingly, the low peak concentrations corresponds to the levels in normal and early AD brains, while the high peak to late AD brains[23].

**Microglial recruitment by human-derived soluble *Aβ*.** To validate the biological relevance of our platform, we measured the microglial response to gradients of soluble *Aβ* enriched or depleted samples derived from tris-buffered saline (TBS) extracts of human AD brains as previously described[24]. For this purpose, low (8 to 20 kDa) and high molecular weight fractions (more than 100 kDa) were separated by size exclusion chromatography (**Fig. 3d**). Both low-molecular-weight soluble *Aβ* (LMW) and high-molecular-weight soluble *Aβ* (HMW) fractions were similar in recruiting microglia towards the central compartment on the eighth day (*R.I.* = 3.7 ± 0.5 for LMW and *R.I.* = 3.9 ± 0.6 for HMW) (**Fig. 3e–f**). Removing the soluble *Aβ* by immune-precipitation considerably reduced the microglial accumulation (*R.I* = 2.7 ± 0.1 for LMW and 2.7 ± 0.7 for HMW), suggesting that a major factor of the TBS extract inducing microglial migration was *Aβ*.

**Self-promoting microglial recruitment by *Aβ*-induced MCP-1 secretion.** Because typical chemotactic responses of various cells display only one activity peak, we investigated further the mechanisms behind the double peak chemotactic activities of microglia in response to *Aβ*. To probe if a second chemoattractant may explain the unusual double chemotactic peak, we utilized a multiplexed cytokine assay to examine 27 cytokines expressed into the media collected from microglia cultured in the presence of soluble $A\beta_{42}$ at 2.3 pg.mL$^{-1}$ for two days. We identified five cytokines at detectable levels: IL-1ra, IL-6, IL-8, MCP-1, and MIP-1b while the remaining cytokines were either below, or just at the threshold of detectability (**Fig. 4a**). Arrows indicate saturated measurement of cytokines relative to the standard curve. Because MCP-1, MIP-1a, and MIP-1b are known chemoattractant molecules for macrophages[3,7,25], we measured microglial recruitment under gradients of soluble $A\beta_{42}$ in addition to a mixture of neutralizing antibodies against MCP-1, MIB-1a, and MIB-1b and observed reduced activity at 23 pg.mL$^{-1}$ but not at 23 ng.mL$^{-1}$ of soluble $A\beta_{42}$ (**Fig. 4c**). In control experiments, we validated that MCP-1 alone can promote microglial recruitment and verified that neutralizing antibodies can reduce microglial recruitment towards the single cytokine (**Fig. 4d**). We further measured the MCP-1 concentration in media from microglia stimulated with various concentrations of both monomeric and oligomeric soluble $A\beta_{42}$. We estimated the maximum secretion of MCP-1 at 1,433.9 ± 816.0 and 1,457.3 ± 109.4 fg.cell$^{-1}$ in the presence of 2.3 pg.mL$^{-1}$ of soluble monomeric and oligomeric $A\beta_{42}$, respectively and 554.4 ± 224.3 fg.cell$^{-1}$ in the absence of soluble $A\beta_{42}$ (**Fig. 4b**). Interestingly, the MCP-1 secretion in the presence of 2.3 pg.mL$^{-1}$ $A\beta_{42}$ was significantly higher than at other concentrations of $A\beta_{42}$ oligomers. While the migration of microglia occurs at higher levels of the gradient (23 pg.mL$^{-1}$) than uniform $A\beta_{42}$ (2.3 pg.mL$^{-1}$), the difference could be explained by the lower effective concentration at the initial region of a gradient. It is possible that MCP-1 plays a role in the peak microglia recruitment activity at a gradient of 23 pg.mL$^{-1}$ soluble $A\beta_{42}$, in addition to other reported roles in microglia-mediated neurodegeneration[26].

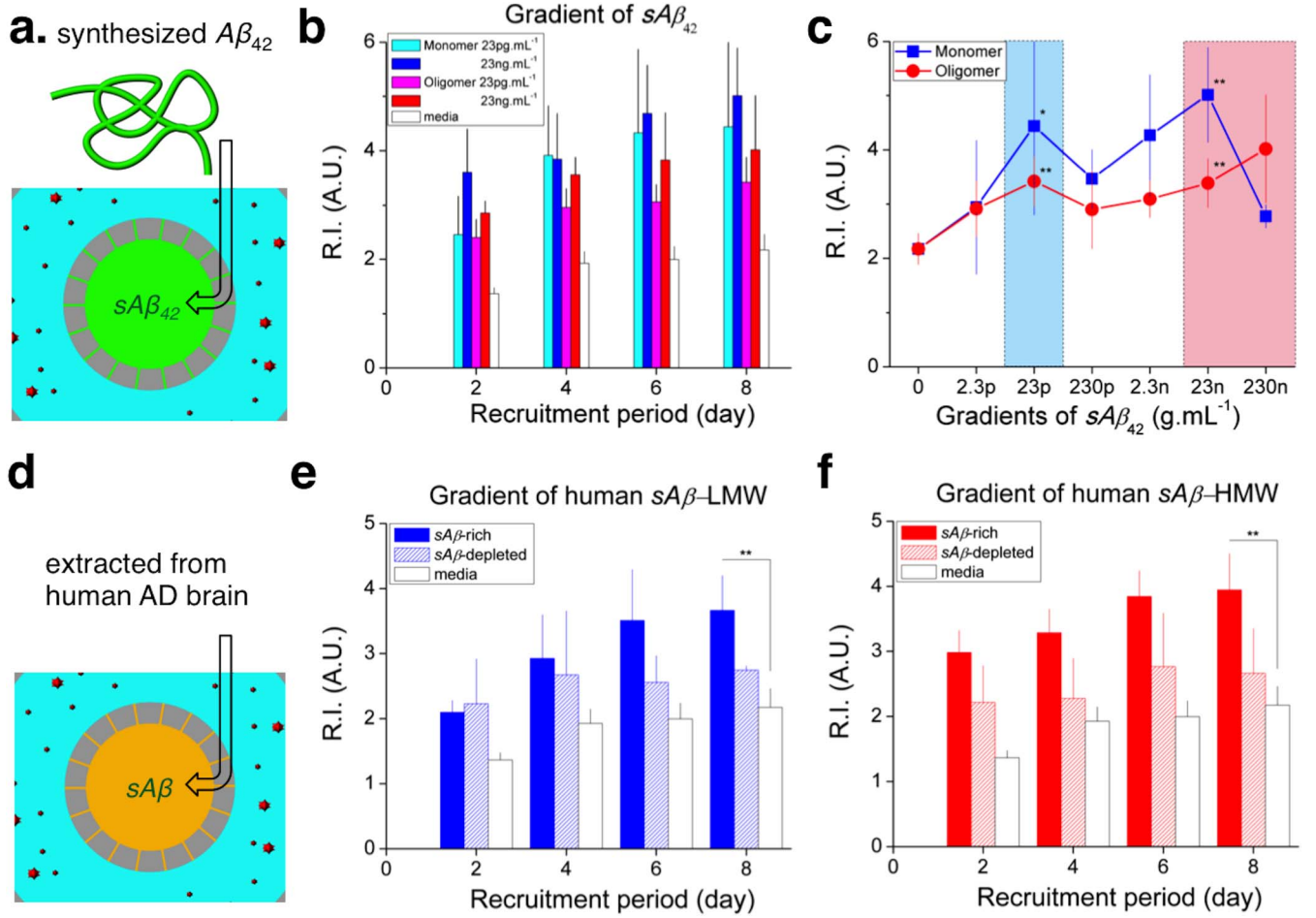


**Figure 3 | Microglial recruitment using various soluble *Aβ*.** (a) Gradients of synthetic $A\beta_{42}$ monomers and oligomers are formed between $A\beta$ reservoir and a microglia hosting annular compartment. (b) Significant recruitment of human primary microglia is measured in the presence of gradients of synthetic $sA\beta_{42}$. (c) Dose-dependence experiments quantified with a recruitment index, *R.I.* on a 'day 8', reveal peak activities under gradients of $sA\beta_{42}$ monomers and oligomers at both concentrations of 23 pg.mL$^{-1}$ and 23 ng.mL$^{-1}$ compatible with measurement of a migration speed in Figure 2. (d) Human $sA\beta$ is extracted from AD brains in low and high molecular weights and forms gradients between $A\beta$ reservoir and a microglia hosting annular compartment. (e), (f) Considerable recruitment of human primary microglia is measured along gradients of human-derived $sA\beta$ at a low molecular weight (LMW) (e) and a high molecular weight (HMW) (f) Immune-depletion of $sA\beta$ from the same human samples results in reduced microglial recruitment effect. (Student's t-test. * $P < 0.1$, ** $P < 0.05$ with respect to no $sA\beta$). $n_{platform} = 4$ and $n_{cell} \approx 2{,}000$ for each condition. Data represent mean ± s.e.m.

**Reduced microglial mobility and viability on *Aβ* fibril-coated surface.** In AD brains, microglia presumably migrate towards plaques, and then remain stably associated with the plaques. To examine the mobility of microglia on surface-bound $A\beta$, we prepared wells uniformly coated with surface-bound $A\beta_{42}$ fibrils and tracked individual microglia cells moving on these surfaces (**Fig. 5a**). We observed that the migration speed of microglia decreased substantially from 26 to 2 μm.hr$^{-1}$ with an increase of surface-bound $A\beta_{42}$ concentration from 9 to 1,125 pg.mm$^{-2}$, consistent with the possibility that surface-bound $A\beta_{42}$ inhibited microglial migration (**Fig. 5b**). We also observed some of the microglia internalizing particles formed on $A\beta_{42}$ fibril–coated surfaces, as well as dead cells (**Supplementary Movies S3, S4**). At the same time, the viability of microglia decreased substantially on highly concentrated surface-bound $A\beta_{42}$. Only 50% of microglia remained viable at 1,125 pg.mm$^{-2}$ after four days, suggesting acute toxicity of surface-bound $A\beta$ fibrils to microglia.

**MCP-1 secretion stimulated by surface-bound *Aβ*.** The level of secreted MCP-1 was elevated also by $bA\beta$ about two-fold (1,128.0 ± 149.8 and 1,088.7 ± 378.2 fg.cell$^{-1}$ under $A\beta$ oligomers and $A\beta$ fibrils at 9 ng.mm$^{-2}$, respectively) compared to without $A\beta$ (554.4 ± 96.0 fg.cell$^{-1}$) (**Fig. 5c**).

**Microglial co-localization with patterned *Aβ*.** To further understand how microglia target surface-bound $A\beta$–rich plaques, we patterned surface-bound $A\beta_{42}$ in both oligomeric and fibril forms on wells at various concentrations by using PDMS stencils of 2 mm holes (**Fig. 5d, Supplementary Fig. S5**). We quantified the co-localization of microglia on the surface-bound $A\beta_{42}$ patterns by calculating a localization index (*L.I.*, defined in **Supplementary Methods**, **Supplementary Fig. S8**), representing the amount of localized cells on the patterned surface-bound $A\beta$ relative to the day of microglia plating. We found that microglia co-localized with surface bound $A\beta_{42}$ patterns at concentrations higher than 45 pg.mm$^{-2}$. We measured a *L.I.* = 1.4 ± 0.1 with oligomers and *L.I.* = 1.9 ± 0.5 with fibrils at 90 pg.mm$^{-2}$ on the eighth day (**Fig. 5e–f**).

**Microglial recruitment and accumulation in the presence of soluble and patterned *Aβ*.** To reconstruct the $A\beta$ microenvironment analogous to that encountered by microglia near plaques, a core of fibrillar $A\beta$ surrounded by a halo of soluble $A\beta$ likely oligomers in the AD brains, we combined patterned surface-bound $A\beta_{42}$ by using PDMS stencils of 1 mm holes and the gradient of soluble $A\beta_{42}$ in the microfluidic platform (**Fig. 5g, Supplementary Fig. S6**). The combination of a gradient of soluble $A\beta_{42}$ oligomers at

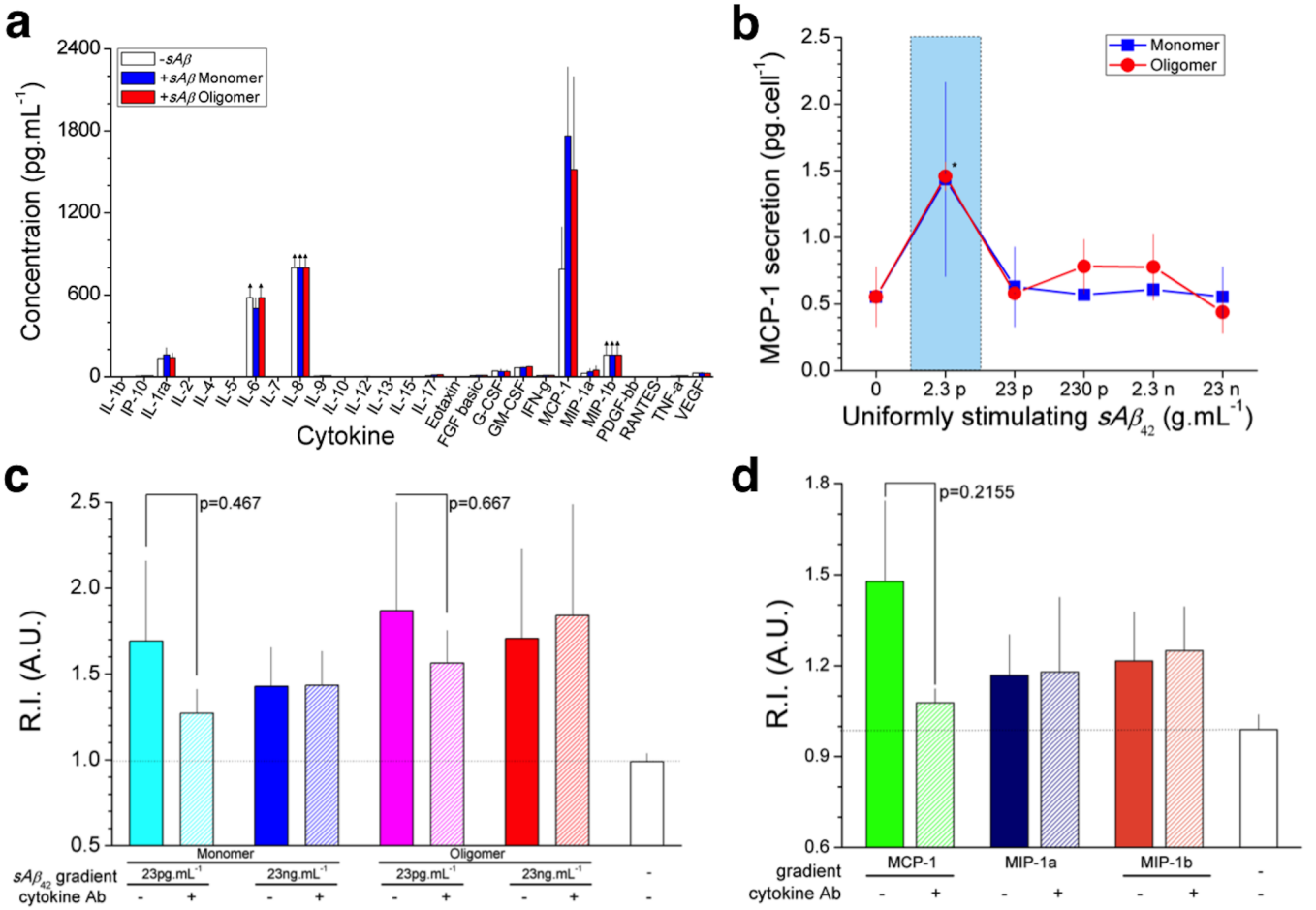


**Figure 4 | MCP-1 secretion from microglia under stimulation of soluble *Aβ* and self-promoted microglial recruitment.** (a) Microglial cells are cultured in wells containing $sA\beta_{42}$ and discernibly expressed five cytokines (MCP-1, MIP-1b, IL-ra1, IL-6, and IL-8) are measured among tested twenty-seven human cytokines from extracted solutions. (b) Highest levels of a cytokine, MCP-1 are measured when microglia are cultured under $sA\beta_{42}$ in monomers and oligomers at 2.3 pg.mL$^{-1}$. (c) Microglial cells are cultured in the presence of gradients of cytokine-neutralizing antibody (Ab) combined with $sA\beta_{42}$ or cytokines and reduction of recruitment index is measured in the presence of neutralizing antibody against MCP-1 and $sA\beta_{42}$ at 23 pg.mL$^{-1}$ but not 23 ng.mL$^{-1}$. (d) MCP-1 is validated to be a potent chemoattractant for microglia and the recruitment is inhibited by immune-neutralization of MCP-1. However, MIP-1a and MIP-1b have no microglial chemoattractant activity in this assay. (Student's t-test. *$P < 0.01$ for oligomers with respect to no $sA\beta_{42}$). $n_{well} = 3$, $n_{cell} \approx 2{,}000$ in '(a)', '(b)' and $n_{platform} = 4$, $n_{cell} \approx 2{,}500$ in '(c)', '(d)' for each condition. Data represent mean ± s.e.m.

5 nM and surface-bound $A\beta_{42}$ fibrils at 90 pg.mm$^{-2}$ achieved the most effective localization by 2.5 times compared to 1.6 ± 0.2 times with surface-bound $A\beta_{42}$ fibrils at 90 pg.mm$^{-2}$ only (**Fig. 5h–i**).

## Discussion

Our study demonstrates that soluble monomeric and oligomeric $A\beta$ serve as a "recruiting signal" and bound fibrillar and oligomeric surface-bound $A\beta$ acts as a "targeting signal" during microglia recruitment and localization. Together, soluble and insoluble $A\beta$ have synergistic effects on microglial accumulation to sites of $A\beta$ deposits, and could explain microglial accumulation in the vicinity of $A\beta$ plaques in the AD cortex.

Moreover, the MCP-1 dependent mechanism of microglia recruitment in response to lower doses of $A\beta$ may be important during physiological neuroinflammation and could be relevant to the early stages of microglial activation in AD. The microfluidic platform can be extended to the study of migration of other cells relevant to the progression of neurodegenerative diseases[27,28], and could help quantify the potency of various cytokines and chemokines, which have been detected in the brain alone and in combinations[11], in modulating microglia recruitment and accumulation. With high-throughput capabilities and regulated microenvironments, our platforms can facilitate systematic monitoring of microglial migration and its modulation by compounds for the treatment of neuroinflammation in various disease conditions, including Alzheimer's disease.

## Methods

**Microfluidic platform fabrication.** Negative photoresists, SU-8 50 and SU-8 100 (MicroChem, Newton, MA, USA), were sequentially patterned using standard lithography on a 4" silicon wafer to create a mold for cell migration channels of 50 μm in height and chemokine compartments of 100 μm in height. A mixture of a base and a curing agent with a 10 : 1 weight ratio (SYLGARD 184 A/B, Dowcorning, Midland, MI, USA) was poured onto the SU-8 mold and cured for one hour at room temperature under vacuum and, subsequently, cured for more than 3 hours in an oven at 80°C. The cured polydimethyl-siloxane (PDMS) replica was peeled off from the mold and holes were punched for fluid reservoirs. Arrayed holes were also laser-cut (Zing 24, Epilog Laser, Golden, CO, USA) into a thin PDMS membrane of 250 μm in thickness (HT 6240, Bisco Silicones, Elk Grove, IL, USA) and an acrylic plate of 6 mm in thickness. The machined membrane and the plate were glued together using uncured PDMS and incubated at 80°C overnight. This assembly was irreversibly bonded first to the PDMS replica using oxygen plasma at 50 mW, 5 ccm, for 30 seconds (PX-250, March Plasma Systems, Petersburg, FL, USA), and later to a glass-bottomed UniWell plate (MGB001-1-2-LG, Matrical Bioscience, Spokane, WA, USA). Immediately after the bonding, 10 μL of poly (l-lysine) solution (PLL, M.W. 70,000–150,000, 1.0 mg.mL$^{-1}$, Sigma-Aldrich Co. LLC, St. Louis, MO, USA) was injected into the each platform and incubated for 2 hours at a room temperature to promote cellular adhesion. PLL-treated surface was rinsed with autoclaved and 0.2 μm filtered water (AM9920, Life Technologies, Grand Island, NY, USA) and then

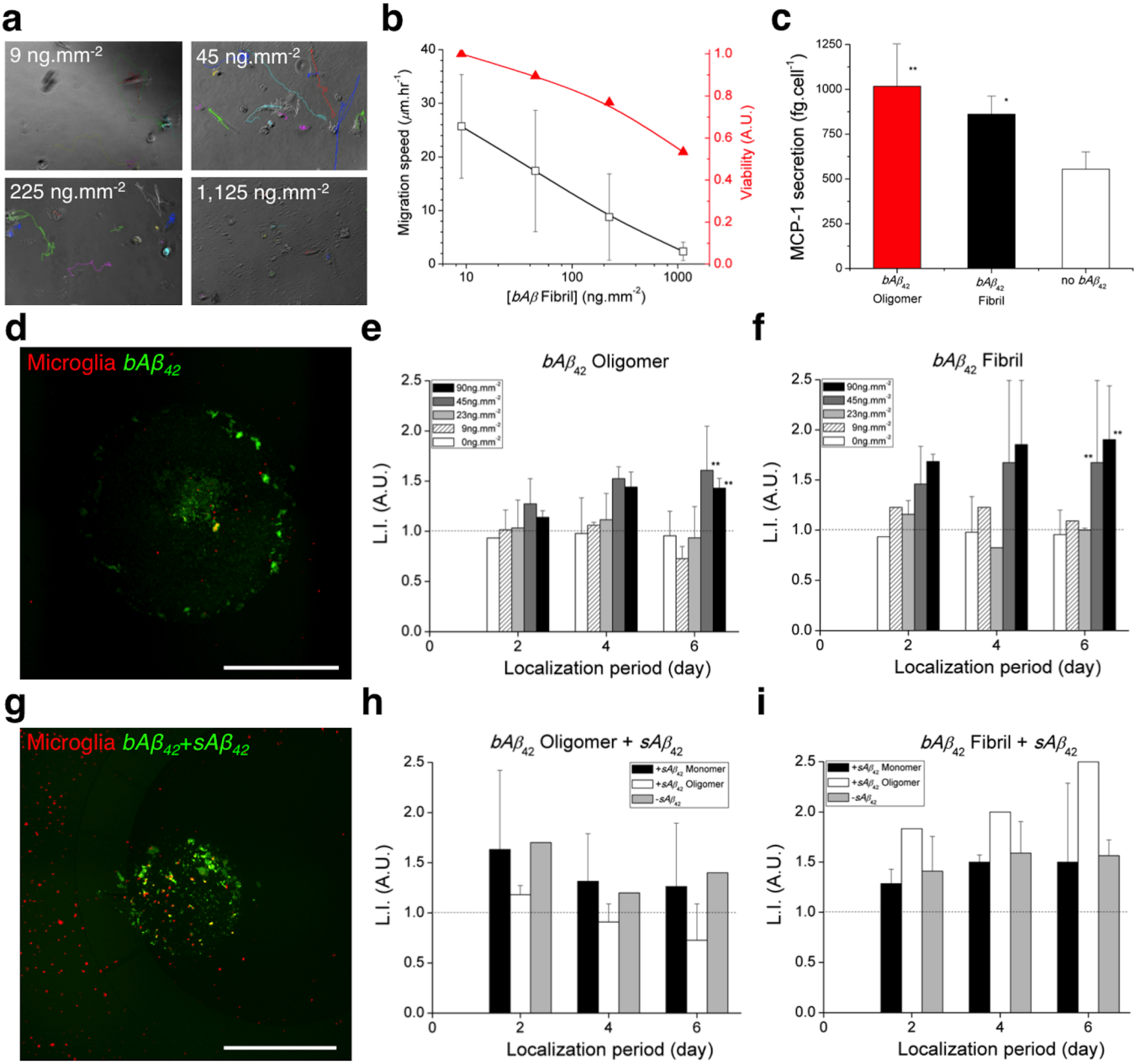


**Figure 5 | Microglial co-localization on surface-bound *Aβ* alone and in combination with soluble *Aβ*.** (a) Microglial cells were cultured in wells uniformly coated with $bA\beta_{42}$ fibrils and tracked individually. (b) The $bA\beta_{42}$ fibrils induce the simultaneous decrease of the mobility and the viability of microglia, proportional to increased concentrations of the $bA\beta$ fibrils. (c) The level of secreted MCP-1 is elevated by about two-fold on surfaces coated with $bA\beta_{42}$ oligomers and $bA\beta_{42}$ fibrils of 9 ng.mm$^{-2}$ compared to an uncoated surface. (d) Fluorescent image visualized co-localized microglia in red on a spot of $bA\beta_{42}$ fibrils at 90 ng.mm$^{-2}$ in green. Co-localization of microglia on the patterned $bA\beta_{42}$, becomes more effective as the concentration increases with 1.5-fold enrichment on $bA\beta_{42}$ oligomers (e) and 2-fold on $bA\beta$ fibrils (f) at 90 ng.mm$^{-2}$ on a 'day 6', respectively. (g) Fluorescent image visualized co-localized microglia on $bA\beta_{42}$ fibrils at 90 ng.mm$^{-2}$ combined with $sA\beta_{42}$ oligomers at 23 ng.mL$^{-1}$ in a microfluidic platform. Co-localization is 1.6-fold on $bA\beta_{42}$ fibrils alone (h) compared to 2.5-fold on $bA\beta_{42}$ fibrils at 90 ng.mm$^{-2}$ in combination with a gradient of $sA\beta_{42}$ oligomers at 23 ng.mL$^{-1}$ (i). Scale bars, 1 mm. (Student's t-test. * $P < 0.1$, ** $P < 0.05$ with respect to no $bA\beta_{42}$). $n_{well} = 2$ in '(a)', '(b)', '(e)', '(f)' and $n_{platform} = 2$, $n_{cell} \approx 2{,}000$ in '(h)', '(i)' for each condition. Data represent mean ± s.e.m.

the devices were filled with cell culture medium containing 50 : 50 of DMEM: F-12 supplemented with 5% FBS (Invitrogen, Grand Island, NY, USA), 10 ng.mL$^{-1}$ of M-CSF (AF-300-25, PeproTech Inc., Rocky Hill, NJ, USA), 25 μg.mL$^{-1}$ of gentamicin (G1397, Sigma-Aldrich), and 2.5 μg.mL$^{-1}$ of amphotericin (A2411, Sigma-Aldrich).

**Cell preparation.** Human microglial cells (HMG 030, Clonexpress, Inc., Gaithersburg, MD, USA) were isolated initially as a free-floating population of cells from fetal brain tissue samples digested with collagenase and grown in a proprietary medium for 1–2 weeks. Before the experiment, cells were washed using medium without serum and the cell membrane was labeled with red fluorescent dye (PKH26PCL, Sigma-Aldrich). After centrifugation (400 *g* for 5 minutes), the cell pellet was re-suspended in 1 mL of Diluent C (G8278, Sigma-Aldrich) and immediately mixed with 4 μL of dye solution (P9691, Sigma-Aldrich) in 1 mL of Diluent C. The cell/dye mixture was incubated at room temperature for 4 minutes and periodically mixed by pipetting in order to achieve a bright, uniform, and reproducible labeling. After the incubation, the staining was stopped by adding an equal volume (2 mL) of 1% BSA in PBS and incubating for 1 minute to remove excess dye. Unbound dye was washed by centrifuging and re-suspending the cells in the culture medium. Finally, the stained microglia cells were suspended in the culturing medium at the concentration of 1 M cells.mL$^{-1}$. Ten μL of cell solution was injected into each platform and 100 μL of a culturing medium was added into side and central extra wells. The loaded cells were incubated at 37°C supplied with 5% $CO_2$ for at least

two days before adding the various $A\beta$ solutions. In the experiments, the cell culture media and $A\beta$ solutions were replaced every two days while collecting the used solutions for $A\beta$ analysis.

**Sourcing of human brain tissue.** Brains from human subjects with a diagnosis of Alzheimer's disease were obtained through the Massachusetts Alzheimer's Disease Research Center. The Massachusetts Alzheimer's Disease Research Center (ADRC) serves, among other clinical and research activities, as a repository of samples from patients with Alzheimer's disease. ADRC clinical and research activities are reviewed among others by the Institutional Review Board at the Massachusetts General Hospital. In addition, the ADRC has a Certificate of Confidentiality issued by the US Department of Health & Human Services/National Institutes of Health to protect the privacy of individuals who are enrolled in this research against forced disclosure in any civil, criminal, administrative, legislative or other proceeding, either at the federal, state of local level. The human samples used in this study were anonymised. The Institutional Review Board at the Massachusetts General Hospital viewed the use of anonymized autopsy material for biochemistry assays as exempt from review.

***Aβ* extraction from human brain tissues.** Cortical gray matter from frontal lobe of AD patient brains was homogenized in 5 volumes of TBSI (Tris-buffered saline with protease inhibitor cocktail (Roche)) with 25 strokes on a mechanical Dounce homogenizer and centrifuged at 260,000 × g for 30 min at 4°C. The supernatant was used as a TBS-soluble fraction[28,29]. 750 μL of TBS-soluble fraction of human brains was separated by a size exclusion chromatography on double superdex 75 columns (GE Healthcare Life Sciences, Piscataway, NJ, USA) in 50 mM ammonium acetate pH 8.5 with an AKTA purifier 10[3,30]. The individual fractions separated by SEC were analyzed by immunoblotting and $A\beta$ specific sandwich ELISA and fraction 6 to 9 (>100 kDa) was used as a HMW $A\beta$ and fraction 30 to 33 (20 ~ 8 kDa) was used as a LMW $A\beta$[30]. Immediately after the size-exclusion chromatography, we removed soluble $A\beta$ including soluble alpha $A\beta$ precursor protein (APP) from the fractions by immune-depleting with 6E10 antibody (Signet, Dedham, MA, USA).

**Time-lapse imaging.** For continuous time-lapse imaging to track individual cells, we kept the UniWell plate on a fully automated microscope (Eclipse Ti, Nikon Inc., Melville, NY, USA) integrated with a heated incubating stage (LiveCell 05-11-0032 Rev B, Pathology Devices Inc., Westminster, MD, USA), which was set at 37.7°C, 5% $CO_2$, and 85% humidity. We imaged cells at every 1-hour (NIS Elements, Nikon Inc.) using a bright field and every 6-hour using a TRITC fluorescence microscope for 4 days with a 10× objective lens and a perfect focusing system in a phase contrast mode. For continual time-lapse imaging to count cells, we kept the plate in an incubation chamber set at 37.7°C and 5% $CO_2$ and then imaged it using 4× objective lens in a large-area mode of 8 × 8 $mm^2$ with a 15% stitching, a phase contrast mode, and a TRITC fluorescent microscope every two–three days for seven days. For continual time-lapse imaging to monitor gradient stability, we kept the plate at room temperature in a dark room, and imaged using 4× objective lens in a large-area mode of 12 × 10 $mm^2$ without stitching, a phase contrast mode, and a TRITC fluorescent microscope every two–three days for nine days.


1. Nakajima, K. & Kohsaka, S. Microglia: activation and their significance in the central nervous system. *J. Biochem.* **130**, 169–175 (2001).
2. Muzio, L., Martino, G. & Furlan, R. Multifaceted aspects of inflammation in multiple sclerosis: the role of microglia. *J. Neuroimmunol.* **191**, 39–44 (2007).
3. Khoury El, J. *et al.* Ccr2 deficiency impairs microglial accumulation and accelerates progression of Alzheimer-like disease. *Nat Med* **13**, 432–438 (2007).
4. Ransohoff, R. M. & Perry, V. H. Microglial physiology: unique stimuli, specialized responses. *Annu. Rev. Immunol.* **27**, 119–145 (2009).
5. Milligan, E. D. & Watkins, L. R. Pathological and protective roles of glia in chronic pain. *Nat. Rev. Neurosci.* **10**, 23–36 (2009).
6. Aguzzi, A., Barres, B. A. & Bennett, M. L. Microglia: scapegoat, saboteur, or something else? *Science* **339**, 156–161 (2013).
7. Nimmerjahn, A., Kirchhoff, F. & Helmchen, F. Resting microglial cells are highly dynamic surveillants of brain parenchyma in vivo. *Science* **308**, 1314–1318 (2005).
8. Hanisch, U.-K. & Kettenmann, H. Microglia: active sensor and versatile effector cells in the normal and pathologic brain. *Nat. Neurosci.* **10**, 1387–1394 (2007).
9. Mawuenyega, K. G. *et al.* Decreased clearance of CNS $\beta$-amyloid in Alzheimer's disease. *Science* **330**, 1774 (2010).
10. Combs, C. K., Karlo, J. C., Kao, S.-C. & Landreth, G. E. $\beta$-amyloid stimulation of microglia and monocytes results in TNF $\alpha$-dependent expression of inducible nitric oxide synthase and neuronal apoptosis. *J. Neurosci.* **21**, 1179–1188 (2001).
11. Xia, M. Q. & Hyman, B. T. Chemokines/chemokine receptors in the central nervous system and Alzheimer's disease. *J. Neurovirol.* **5**, 32–41 (1999).
12. Serrano-Pozo, A. *et al.* Stable size distribution of amyloid plaques over the course of Alzheimer disease. *J. Neuropathol. Exp. Neurol.* **71**, 694–701 (2012).
13. Bolmont, T. *et al.* Dynamics of the microglial/amyloid interaction indicate a role in plaque maintenance. *J. Neurosci.* **28**, 4283–4292 (2008).
14. Grathwohl, S. A. *et al.* Formation and maintenance of Alzheimer's disease beta-amyloid plaques in the absence of microglia. *Nature Neuroscience* **12**, 1361–1363 (2009).
15. Meyer-Luehmann, M. *et al.* Rapid appearance and local toxicity of amyloid-$\beta$ plaques in a mouse model of Alzheimer's disease. *Nature* **451**, 720–724 (2008).
16. Takata, K. *et al.* Microglial transplantation increases amyloid-$\beta$ clearance in Alzheimer model rats. *FEBS Lett.* **581**, 475–478 (2007).
17. Burguillos, M. A. *et al.* Caspase signalling controls microglia activation and neurotoxicity. *Nature* **472**, 319–324 (2011).
18. Grienberger, C. *et al.* Staged decline of neuronal function *in vivo* in an animal model of Alzheimer's disease. *Nat. Comm.* **3**, 774 (2012).
19. Koffie, R. M. *et al.* Apolipoprotein E4 effects in Alzheimer's disease are mediated by synaptotoxic oligomeric amyloid-$\beta$. *Brain* **135**, 2155–2168 (2012).
20. Hosmane, S., Yang, I. H., Ruffin, A., Thakor, N. & Venkatesan, A. Circular compartmentalized microfluidic platform: study of axon–glia interactions. *Lab on a Chip* **10**, 741–747 (2010).
21. Taylor, A. M. *et al.* A Microfluidic culture platform for CNS axonal injury, regeneration and transport. *Nat. Methods* **2**, 599–605 (2005).
22. Kim, S., Kim, H. J. & Jeon, N. L. Biological applications of microfluidic gradient devices. *Integr Biol (Camb)* **2**, 584–603 (2010).
23. Fagan, A. M. *et al.* Decreased cerebrospinal fluid $A\beta_{42}$ correlates with brain atrophy in cognitively normal elderly. *Annals of Neurology* **65**, 176–183 (2009).
24. Wu, H.-Y. *et al.* Amyloid beta induces the morphological neurodegenerative triad of spine loss, dendritic simplification, and neuritic dystrophies through calcineurin activation. *J. Neurosci.* **30**, 2636–2649 (2010).
25. Ishizuka, K. *et al.* Identification of monocyte chemoattractant protein-1 in senile plaques and reactive microglia of Alzheimer's disease. *Psychiatry Clin Neurosci* **51**, 135–138 (1997).
26. Yang, G. *et al.* Neuronal MCP-1 mediates microglia recruitment and neurodegeneration induced by the mild impairment of oxidative metabolism. *Brain Pathol.* **21**, 279–297 (2011).
27. Franciosi, S., Choi, H. B., Kim, S. U. & McLarnon, J. G. IL-8 enhancement of amyloid-beta ($A\beta$ 1-42)-induced expression and production of pro-inflammatory cytokines and COX-2 in cultured human microglia. *J. Neuroimmunol.* **159**, 66–74 (2005).
28. Fuhrmann, M. *et al.* Microglial Cx3cr1 knockout prevents neuron loss in a mouse model of Alzheimer's disease. *Nat. Neurosci.* **13**, 411–413 (2010).
29. Hashimoto, T. *et al.* CLAC: a novel Alzheimer amyloid plaque component derived from a transmembrane precursor, CLAC-P/collagen type XXV. *EMBO J.* **21**, 1524–1534 (2002).
30. Townsend, M., Shankar, G. M., Mehta, T., Walsh, D. M. & Selkoe, D. J. Effects of secreted oligomers of amyloid $\beta$-protein on hippocampal synaptic plasticity: a potent role for trimers. *J. Physiol.* **572**, 477–492 (2006).


## Acknowledgments

This work was supported in part by funding from the National Institutes of Health, grants AG005134 – pilot project 27.3, GM092804 and EB002503. We thank the BioMEMS RC for the use of fabrication facilities, Dr. Salil Desai for advise on microscale patterning techniques, and Dr. Ken Arai for discussion of $A\beta$ stability.

## Author contributions

H.C., L.Z., B.T.H. and D.I. conceived the microfluidic platforms. H.C. and T.H. performed experiments and analysed data. T.H. prepared and analyzed human-derived soluble $A\beta$. H.C. and E.W. developed the algorithms for analyzing microglial mobility. Y.H. executed ELISA, western blot assays, EM imaging, and analyzed data. L.B.W. and K.M.H. executed a multiple cytokine assays and analyzed data. H.C., L.B.W., B.T.H. and D.I. wrote the manuscript.

## Additional information

**Supplementary information** accompanies this paper at http://www.nature.com/scientificreports

**Competing financial interests:** The authors declare no competing financial interests.



**How to cite this article:** Cho, H. *et al.* Microfluidic Chemotaxis Platform for Differentiating the Roles of Soluble and Bound Amyloid-$\beta$ on Microglial Accumulation. *Sci. Rep.* **3**, 1823; DOI:10.1038/srep01823 (2013).